GAP MEASUREMENT IN Nb/NbO_X/Al INJECTION CONTROLLED PLANAR THREE TERMINAL DEVICES

Kiyoshi Takeuchi and Yoichi Okabe

Dept. of Electronic Engineering, the University of Tokyo, Bunkyo-ku, Tokyo 113, JAPAN

Abstract

Characteristics of Nb/NbO_X/Al injection controlled planar three terminal superconducting devices (injection controlled links) have been studied experimentally. A built-in Nb/AlO_X/Nb Josephson junction is used to perform direct tunneling measurement, whose results show that the gap in the Nb strip decreases according as its critical current is suppressed. It is also shown that the static characteristics of the devices with high and low injector resistance can be fitted to a simple heating model and a modified heating model respectively.

Introduction

There is a category of three terminal superconducting devices in which the critical current of a superconducting strip is controlled by quasiparticle injection.[1-6] Although such 'injection controlled links' have mainly been investigated from the viewpoint of making Josephson weak links with tunable characteristics, the devices seem to be even more attractive as a superconducting switching element, since they are unique in their high current gain, large output voltage and structural simplicity.

It is believed that the critical current modulation in the injection controlled links is due to a suppression of the order parameter induced by the quasiparticle injection. However, since energy gap measurement in these devices had not been achieved, it is still unclear how the critical current and the order parameter are related. Hence, we have attempted to make direct gap measurement using Nb/Al injection controlled links. In this paper, we report on their static characteristics, including the results of the gap measurement.

Device Structure and Fabrication Process

We have fabricated two types of Nb/NbO_X/Al injection controlled links: type A (with a gap detector) and type B (without a gap detector), which are illustrated in Fig. 1. Basically, the devices consist of an Al strip crossing upon a Nb strip with a NbO_X barrier sandwiched between them, where the critical current of the Nb strip is controlled by the current injected from the Al electrode. In addition, the type-A devices comprise a built-in Nb/AlO_X/Nb Josephson junction (detector junction) placed immediately beneath the Nb/NbO_X/Al junction, so that any gap modulation induced by the current injection can be detected.

Fabrication process for the type-A devices is shown in Fig. 2. First, the detector junction is formed in-situ on a thermally oxidized Si substrate by depositing 170 nm of Nb and 6 nm of Al, thermally oxidizing the Al in 100 Pa pure oxygen, and depositing again 20 nm of Nb. Then, the junction length is defined using selective niobium anodization technique[7] (Fig. 2a). A layer of 70 nm-thick Nb is deposited onto the Nb/AlO_X/Nb junction and patterned with a reactive ion etching (RIE) apparatus. Selective anodization is again performed without removing the photoresist used

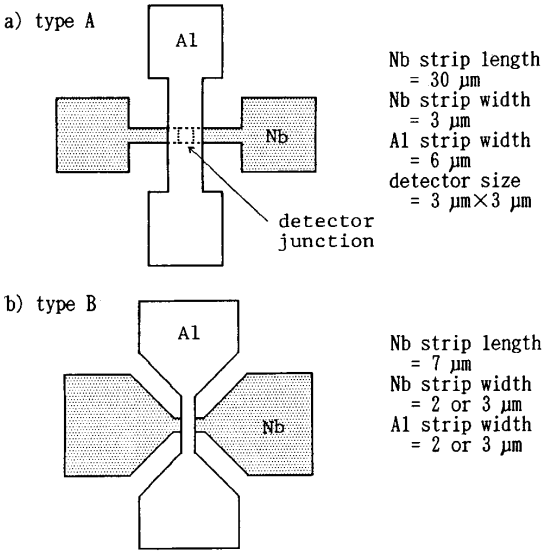

Fig. 1 Device structure.

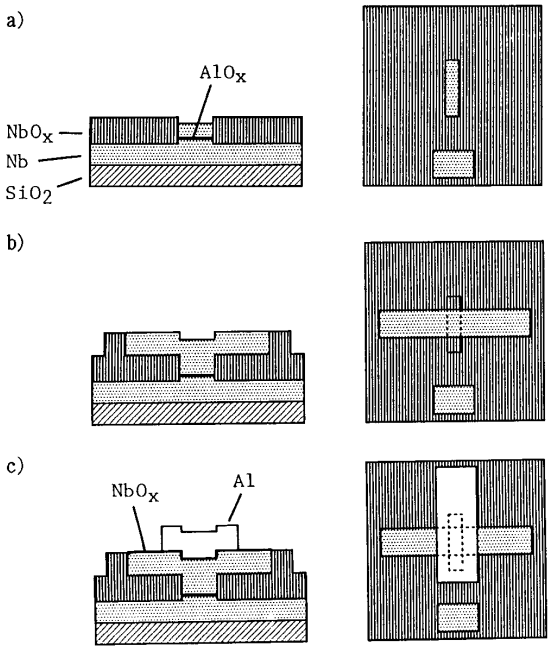

Fig. 2 Fabrication process for the type-A devices.

Manuscript received August 22, 1988.

as the etching mask; this step insulates the sides of the Nb strip and defines the detector junction width self-aligned to the Nb strip (Fig. 2b). Then, the surface of the Nb strip is thermally oxidized in air to form an oxide tunnel barrier, and finally, 170 nm of Al is evaporated onto the Nb strip and patterned by using lift-off technique (Fig. 2c). All the metal layers were deposited using an electron beam evaporator with the substrates being water-cooled.

Fabrication process for the type-B devices is similar to the latter part of the type-A process, except that the anodization steps were omitted. Samples without any NbO_x layer were also prepared using Ar plasma cleaning prior to the Al deposition.

Experimental Results

Figure 3 shows the current-voltage (I-V) characteristics of a typical type-B $Nb/NbO_x/Al$ device having a 2 μm square injector junction. The measurement was made at 4.2 K immersing the sample in liquid He. Without any injection from the Al electrode, the critical current (I_C) of the Nb strip is as large as 37 mA, and the I-V curve is hysteretic presumably due to the Joule heating produced by the bias current (Fig. 3a). As the injection current (I_g) is increased up to 1.03 mA, I_C decreases continuously to zero. When I_g gets close to 1.03 mA, the I-V curve becomes non-hysteretic (Fig. 3b). Under such conditions, rf-induced constant voltage steps are observed (Fig. 3c). The I-V curves of the type-A devices are similar to those of the type-B ones.

Various parameters of the devices used in this work are listed in Table I. The injector resistance of the type-A samples has become high because the photoresist mask against the anodization was imperfect, while that of the type-B ones is relatively low. Both high and low injector resistance samples show critical current modulation, but the samples without a NbO_x barrier (samples c1 and c2) do not exhibit any modulation. It should also be noted that the injected power per unit volume required to suppress the supercurrent completely is almost identical irrespective of the injector resistance. This means that the current or the voltage gain can be adjusted by varying the injector resistance.

Figure 4 shows the detector I-V curves of one of the type-A devices at 4.2 K with various amounts of current injected from the Al electrode. The curves are displaced along the current axis for clarity. It can be seen that the sum gap voltage ($\Delta 1+\Delta 2$) is suppressed by the current injection around 100 μA, while an injection current of 140 μA was required to suppress the supercurrent of the Nb strip for the same sample. This result clearly shows that the I_C modulation in the type-A samples is accompanied by a gap modulation. This fact strongly supports the widely accepted assumption that the critical current modulation in injection controlled links arises from a gap modulation.

We will compare the experimental results with two nonequilibrium models in which the energy distribution functions of quasiparticles and phonons are assumed to take simple analytic forms: a simple heating model and a modified heating model.[8] The simple heating model

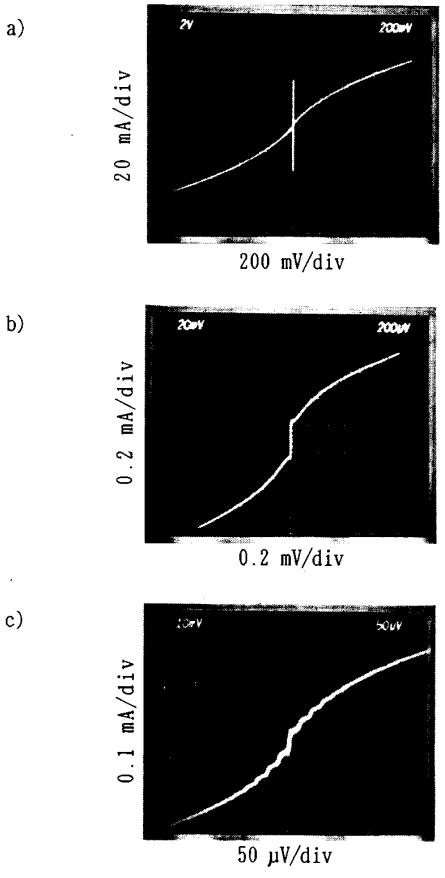

Fig. 3. I-V characteristics of sample b2; a) Ig=0, b) Ig=1.0 mA, and c) Ig=0.97 mA with microwave (10 GHz) irradiated.

Table I. Basic parameters of the samples used in this work; W is the width of the Nb strip, L the width of the Al strip, I_C the critical current of the Nb strip, V_{gc} and I_{gc} are the injector voltage and current respectively required to drive I_C to zero, $P_C=V_{gc}\times I_{gc}$, and $V=W\times L\times 70$[nm]. The measurement was made at 4.2[K].

sample	type	W [μm]	L [μm]	I_C [mA]	V_{gc} [mV]	I_{gc} [mA]	P_C/V [μW/μm3]
a1	A	3	6	30.0	308.	0.14	34.
a2	A	3	6	11.8	312.	0.12	30.
b1	B	3	3	44.5	10.5	2.1	35.
b2	B	2	2	37.0	9.1	1.0	33.
b3	B	2	2	27.5	9.6	1.2	41.
c1	B	3	3	36.0	-	-	-
c2	B	2	2	32.0	-	-	-

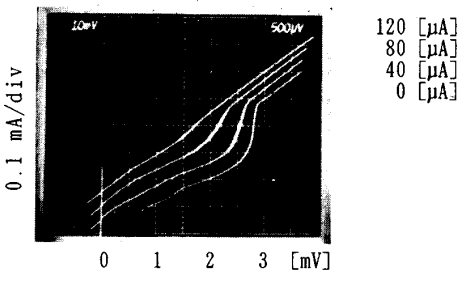

Fig. 4. Detector I-V curves of sample a1 with injector currents Ig=0, 40, 80, and 120 μA. The curves are shifted along the current axis.

assumes that the power injected into a superconductor simply raises the temperature, keeping the distribution functions in complete thermal equilibrium. Then, assuming a Debye-like phonon density of states, and neglecting the heat flow along the films, the injected power (P_i) and the temperature (T) under injection are related by

$$P_i = C\,(T^4 - T_b^4) \equiv \frac{U_{ph}(T) - U_{ph}(T_b)}{\tau_{es}}, \qquad (1)$$

where C is a constant, $U_{ph}(T)$ the total energy of the phonons in the superconductor, T_b a bath temperature, and τ_{es} the effective escape time of the phonons through the boundaries of the superconductor. Here, heating of the Al electrode is also accounted for. In the modified heating model, or T* model, it is assumed that quasiparticles and those phonons with energy larger than 2Δ are characterized by their thermal equilibrium distribution functions at an elevated temperature T^*, while the distribution of the rest of the phonons remains unchanged. Combining this assumption with Rothwarf-Taylor equations, which are a pair of rate equations for quasiparticles and the phonons with energy higher than 2Δ, one obtains

$$P_i = \frac{2\,N_{ph}(T_b)\,E_{qp}(T^*)}{\tau_{es}\,F(T^*)}\left(\frac{N_{qp}(T^*)^2}{N_{qp}(T_b)^2} - 1\right), \qquad (2)$$

where $N_{ph}(T)$ is the number of the phonons with energy higher than 2Δ, $N_{qp}(T)$ the number of the quasiparticles, $E_{qp}(T)$ the average energy of a quasiparticle, and $F(T)$ the fraction of the injected energy that is shared among the quasiparticles. In Eqs. (1) and (2), quasiparticle and phonon diffusion are not considered. In both models, power dependence of the energy gap can be obtained using either Eq. 1 or Eq. 2 and the BCS temperature-gap relation.

First, we compare with the models the experimental I_C-P_i relation of the type-A samples. To do this, we need some method to relate I_C with Δ. In this connection, we measured the gap and the critical current, varying the temperature (T) as a parameter between 4.2 K and the critical temperature (T_C=8.5 K). It was confirmed that the temperature dependence of the gap determined from the detector I-V curve of the type-A samples can quite well be fitted to the standard BCS relation. It was also found that I_C in the type-A and type-B samples is proportional to the third power of $\Delta(T)$ not only when T is close to T_C but over the full measurement temperature range, where $\Delta(T)$ is the theoretical BCS gap at a measurement temperature T. Hence, we assume

$$\Delta \propto I_c^{1/3}, \qquad (3)$$

which is at least justified in the thermal equilibrium conditions. In Fig. 5, Δ derived from the measured I_C is plotted as a function of P_i, where P_i is assumed to be a fixed proportion of the total power $I_g \times V_g$ generated by the injection current. The solid line is the prediction of the simple heating model, which is in excellent agreement with the experimental data.

In Fig. 6, the measured sum gap energy of the type-A samples at various injection levels is plotted against $I_C^{1/3}$ for the same injection current. The gap energy on the vertical scale is not that of the Nb strip alone (say Δ_1), but the sum of Δ_1 and the gap of the detector electrode ($\Delta_1+\Delta_2$), since we could not detect the gap difference signal due to subharmonic gap structure. If Δ_2 is not perturbed by the injection at all and Eq. 3 holds true, the data are expected to fit the dashed straight lines. However, the measured data slightly diverge downward from the lines, probably because Δ_2 is suppressed by the injection as well as Δ_1. To explain this discrepancy, we assume that the heat flow between the Nb strip and the substrate is separated into two stages which are given as

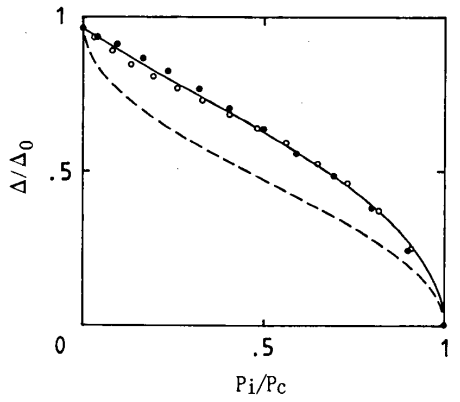

Fig. 5. Gap Δ derived from measured I_C vs. injected power P_i for the type-A samples. The solid and the dashed curves are the predictions of the simple heating model and the modified heating model respectively.

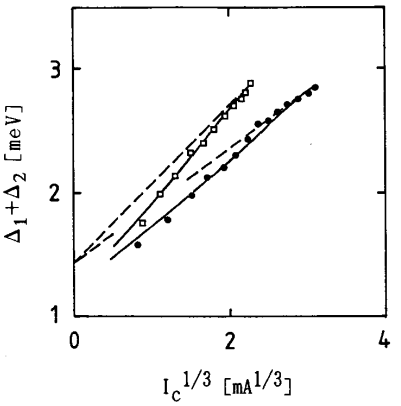

Fig. 6. Measured sum gap energy $\Delta_1+\Delta_2$ vs. $I_C^{1/3}$ for the type-A samples. The solid and the dashed lines are the theoretical curves for $C_1/(C_1+C_2)=0$ and 0.2 respectively.

$$P_{os} = C_1\,(T^4 - T_d^4) = C_2\,(T_d^4 - T_b^4), \qquad (4)$$

where P_{os} is the power that flows out into the substrate, T_d the temperature of the detector electrode, and C_1 and C_2 are constants corresponding to the heat transmission through the strip-detector and the detector-substrate interface respectively. The solid curves in Fig. 6 are the theoretical curves for $C_1/(C_1+C_2)=0.2$, which well fit the experimental data.

Figure 7 shows the same kind of data as Fig. 5 for the type-B samples which have low injector resistance. The solid curve is the prediction of the modified heating model described by Eq. 2, where $F(T)$ was chosen according to Parker,[8] and $F(T=0)=1$ and $F(T=T_C)=0.4$ for Nb. The experimental data fit the modified heating curve, which is apparently different from the simple heating curve to which the type-A samples are fitted. Such difference would reflect the difference in the energy distribution of the injected

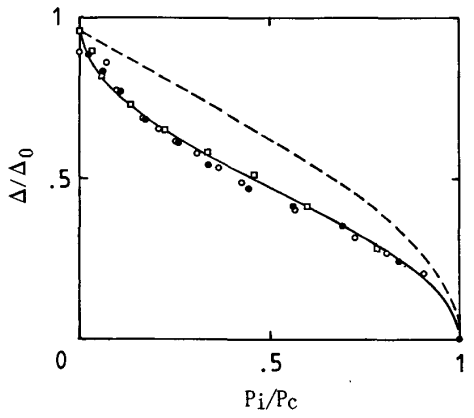

Fig. 7. A similar graph as Fig. 5 for the type-B samples. The solid and the dashed curves are the predictions of the modified heating model and the simple heating model respectively.

quasiparticles. Although the experimental data fit the modified heating curve, we do not insist that the model explains the experimental results, since, unlike the simple heating model, the modified heating model includes an uncertain parameter F(T), to which the shape of the curve is rather sensitive. For instance, if F is a constant, the theoretical curve lies in the middle of the two curves in Figs. 5 or 7. For the full understanding of the results, more detailed calculation and more careful experiment will be required.

Discussion

In Eqs. 1 and 2, heat or quasiparticle diffusion terms are neglected. To estimate the effect of such terms, we have made numerical calculations using a modified version of Eq. 1:

$$P_i(x) = C\,(T(x)^4 - T_b^4) - K\,\frac{\partial^2 T(x)}{\partial x^2}, \qquad (5)$$

where K is a thermal conductivity. The parameter C was determined from the observed modulation characteristics of the type-A samples using Eq. 1. The thermal conductivity K was roughly estimated from the measured electrical conductivity of our Nb film (3.5×10^6 S/m) using the Wiedemann-Franz law. Considering the worst case, a sample geometry with a 2 μm-wide injector electrode was assumed. The results show that the power required to drive the Nb film normal at the center of the injector electrode is about 10 percent larger than for the case with no diffusion. However, it was found that the shape of the P_i-Δ curve is very little affected by the diffusion term.

We can roughly estimate the effective phonon escape time τ_{es} by fitting the static characteristics of the devices to Eqs. 1 or 2. Then, an effective phonon transmissivity η can be obtained using the relation

$$\tau_{es} = 4\,d\,/\,\eta\,c_s, \qquad (6)$$

where d is the film thickness and c_s an average sound velocity. For our type-A samples, τ_{es} and η are estimated to be approximately 0.7 ns and 0.17 if the half of the injector power is assumed to be injected into the Nb side.

Conclusion

We have fabricated Nb/Al injection controlled links, where the critical current of the Nb strip (I_c) is suppressed by injecting small current from the Al strip crossing upon it. By means of the direct tunneling measurement, it was found that, at least in the high injector resistance samples (max injection voltage = 300 mV), the gap in the Nb strip decreases according as its I_c is suppressed by the current injection. The relation between I_c and the injected power (P_i) for these samples is in good agreement with the predictions of the simple heating model. The measured modulation rate of the sum gap also agrees with the model qualitatively. In the low injector resistance samples (max injection voltage = 10 mV), the shape of the I_c-P_i relation is different from that in the high resistance ones, and can be fitted to the modified heating model, which result probably reflects the difference in the quasiparticle energy distribution. However, in spite of this discrepancy, the power per unit volume required to suppress the supercurrent completely is almost a constant irrespective of the injector resistance.

Acknowledgment

The authors wish to thank Dr. T. Sugano for his encouragement.

References

[1] Ting-wah Wong, J. T. C. Yeh, and D. N. Langenberg, "Quasiparticle-Injection-Induced Superconducting Weak Links," Phys. Rev. Lett. 37, 150-153, 1976.
[2] Ting-wah Wong, J. T. C. Yeh, and D. N. Langenberg, "Controllable Superconducting Weak Links," IEEE Trans. Mag. MAG-13, 743-746, 1977.
[3] S. B. Kaplan, "Simple-heating-induced Josephson effects in quasiparticle-injected superconducting weak links," J. Appl. Phys. 51, 1980.
[4] S. Sakai and H. Tateno, "Quasiparticle-Injected Superconducting Weak Link Device," Jap. J. Appl. Phys. 21, Suppl. 21-1, 331-336, 1982.
[5] K. Kojima, S. Nara, and K. Hamanaka, "Thin-film dc SQUID consisting of quasiparticle-injected superconducting weak links," Appl. Phys. Lett. 47, 325-327, 1985.
[6] Y. Okabe, P. Anprung, and K. Fukuoka, "Superconductive Controlled Weak-Links," Jap. J. Appl. Phys. 25, 1342-1347, 1986.
[7] H. Kroger, L. N. Smith, and D. W. Jillie, "Selective niobium anodization process for fabricating Josephson tunnel junctions," Appl. Phys. Lett. 39, 280-282, 1981.
[8] W. H. Parker, "Modified heating theory of nonequilibrium superconductors," Phys. Rev. B12, 3667-3672, 1975.